An Ab initio investigation of ultra-low thermal conductivity in organically functionalized TaS_2.

*Francesco Siddi Antonio Cappai Luciano Colombo Claudio Melis**

Department of Physics, University of Cagliari, Monserrato, Italy: Francesco Siddi, Antonio Cappai, Luciano Colombo, Claudio Melis*
Email Address:claudio.melis@dsf.unica.it

Keywords: *transition metal dichalcogenides, thermal transport, organic functionalization, thermoelectricity*

An *ab-initio* characterization of the impact of tert-Butyl isocyanate (C_5H_9NO) functionalization on TaS_2 lattice thermal conductivity is presented. Such a system is experimentally synthetized showing that the incorporation of covalently bonded C_5H_9NO on bulk TaS_2 leads to a dramatic in-plane lattice thermal conductivity decrease by more than two orders of magnitudes. To elucidate these experimental findings, detailed calculations of the phonon dispersion relations and scattering rates in TaS_2 are performed. The analysis is addressed to discern the impact of inter-layer covalently bonded C_5H_9NO molecules on these phonon properties, providing insights into the underlying mechanisms of the observed thermal conductivity decrease. The findings show that the observed lattice thermal conductivity reduction is attributed to two effects: *i*) the increase of inter-layer separation and *ii*) the presence of low-frequency molecular optical modes. The first inhibits specific Van der Waals quasi-acoustic inter-layer vibrational modes contributing as much as ≈55% in bulk TaS_2. The second effect dramatically decreases the phonon group velocities as a consequence of phonon-crossing phenomena among low-frequency molecular modes and TaS_2 acoustic modes, eventually leading to a strong reduction of all phonon lifetimes.

1 Introduction

Improving and expanding the capabilities of 2D materials has emerged as a focal point in scientific research [1, 2]. This focus is motivated by their distinctive layered structures, which impart substantial advantages in electronic, mechanical, and thermal properties. Apart from graphene, during recent years, various 2D materials have been successfully characterized and experimentally fabricated [3]. Among the hundreds of available 2D materials, transition metal dichalcogenides (TMDCs) have recently gained a central role in many research fields [4]. Defined by the formula MX_2, with M denoting a transition metal (TM) atom ranging from group IV to V, and X representing a chalcogen atom (S, Se, or Te), TMDCs such as molybdenum disulfide (MoS_2), tungsten disulfide (WS_2), and tungsten diselenide (WSe_2) have attracted huge attention. The layered structure of TMDCs, depicted as X–M–X, introduces a plane of metal atoms separating the two hexagonal planes of chalcogenides, offering a distinctive structural arrangement. With over forty different combinations of multi-layered elements within the TMDC family, diverse TM and chalcogen atom blends contribute to their composition [5]. TMDCs exhibit either trigonal prismatic (2H) or octahedral (1T) coordinations, distinguishing them from graphene due to the presence of a bandgap in their mono-layer state. Significantly, the semiconducting properties of TMDCs undergo a crucial transformation as they transition from bulk to mono-layer configurations, shifting their band gap from indirect to direct [6].
The versatile electronic properties, coupled with mechanical flexibility and optical sensitivity [7], set TMDCs as candidates for a diverse array of applications. These include semiconductor systems, lightweight wearables, and flexible technologies. For instance, a MoS_2 transistor can achieve a carrier mobility of up to 200 $cm^2V^{-1}s^{-1}$ [8]. High-performance light-emitting transistors and field-effect transistors based on MoS_2 [9] and WS_2 have also been produced [10].
In most of the TMDCs' applications, thermal properties play a pivotal role in determining the device performance [11]. For example, efficient heat dissipation in high-performance electronic devices demands a high thermal conductivity [12], while thermoelectric applications request a lower thermal conductivity [13]. For this reason it is crucial to develop effective strategies to properly tune the TMDCs' thermal conductivities. Classical thermal transport theory suggests that due to heavy atom mass TMDC sheets

exhibit low thermal conductivities. Therefore, mono- or few-layer TMDCs sheets are considered potential thermoelectric materials. However, the reported experimental values of thermal conductivities typically show large values, e.g., MoS_2 (52 $cm^2V^{-1}s^{-1}$ [14]),$MoSe_2$ (44 $cm^2V^{-1}s^{-1}$ [15]), TaS_2 (36 $cm^2V^{-1}s^{-1}$ [16]), $TaSe_2$ (16 $cm^2V^{-1}s^{-1}$ [17]), at room temperature. For this reason, pristine TMDCs are currently considered not mature yet for thermoelectric applications even if they present remarkable electrical conductivity and Seebeck coefficient.
A recent exploration has unveiled a potential strategy to decrease the thermal conductivity of TMDCs without affecting their corresponding thermoelectric power factor, as documented by Wang et al. [16]. Notably, the incorporation of covalently bonded organic side-chains, such as tert-Butyl isocyanate (C_5H_9NO), leads to a dramatic decrease in the in-plane lattice thermal conductivity by almost two orders of magnitude. Simultaneously, this modification results in slight enhancements in both electrical conductivity and the Seebeck coefficient. This issue sets the TaS_2+C_5H_9NO system as a highly promising candidate for thermoelectric applications. Similar strategies have previously proven successful in organic crystals, demonstrating that the introduction of suitable side chains can significantly influence the thermal transport properties [18, 19].
Although the experimental results confirm a significant reduction, the exact impact of functionalizing TMDCs with organic molecules on their thermal properties is not thoroughly characterized. For this reason a full atomistic investigation is crucial to understand the mechanisms underlying this observed phenomenon and its implications for the material thermal properties in practical applications. Specifically, the experimental findings highlight that the functionalization of TaS_2 with organic molecules resulted in an increased distance between the TaS_2 layers. This underscores the critical necessity to examine whether the observed reduction in lattice thermal conductivity is attributed to this separation or influenced by some explicit effect of the vibrational degrees of freedom of the organic molecules. In contrast to other 2D materials like graphene [**?**, 20] and BN [21], all the TMDCs exhibit a general reduction in thermal conductivity from bulk to mono-layers [17, 22, 23]. Furthermore, the impact of covalently bonded organic molecules on the vibrational (both harmonic and anharmonic) properties, as well as the thermal properties of 2D materials, remains incompletely characterized.
To elucidate the specific role played by organic molecules in this phenomenon, we performed a thorough ab initio analysis aimed at assessing the impact of covalently bonded organic side-chains on the thermal properties of TaS_2, encompassing both harmonic and anharmonic vibrational properties.
The outcomes of our investigation underscore a notable reduction in thermal conductivity, attributing this phenomenon to a combination of two factors. A significant contribution is the increase of inter-layer distance induced by the presence of organic molecules. This increase in separation exerts an influence by decreasing the thermal conductivity through the disappearance of specific shearing inter-layer vibrational modes. The second contribution is indeed attributed to the physical presence of covalently bonded organic molecules. Specifically, the existence of low-frequency molecular optical modes prompts a corresponding reduction in TaS_2 acoustic modes group velocities, ultimately leading to an overall decrease in thermal conductivity.

2 Results and discussion

It has been already highlighted that the functionalization of TaS_2 with tert-Butyl isocyanate has two notable effects. First, a significant increase in the inter-layer distance, from 6.03 to 10.36 Å, is observed. Second, this process results in the formation of a covalent bond between the carbon atom of the isocyanate group and a sulfur atom of TaS_2. The synergy between these structural and chemical modifications is crucial, leading to a remarkable 60-fold reduction in lattice thermal conductivity. To decipher the origin of such a remarkable reduction, we performed a very careful analysis of the vibrational properties of three representative structures, each obtained through a very accurate geometry optimization (see the methodological section for technical details), namely: *a*) bulk TaS_2 (see Figure 1, left); *b*) elongated TaS_2 (see Figure 1, center); *c*) functionalized TaS_2 (see Figure 1, right). The optimized structure (*a*) show an inter-layer distance of 6.02 Å and a cell angle of 90° that are in perfect agreement with the correspond-

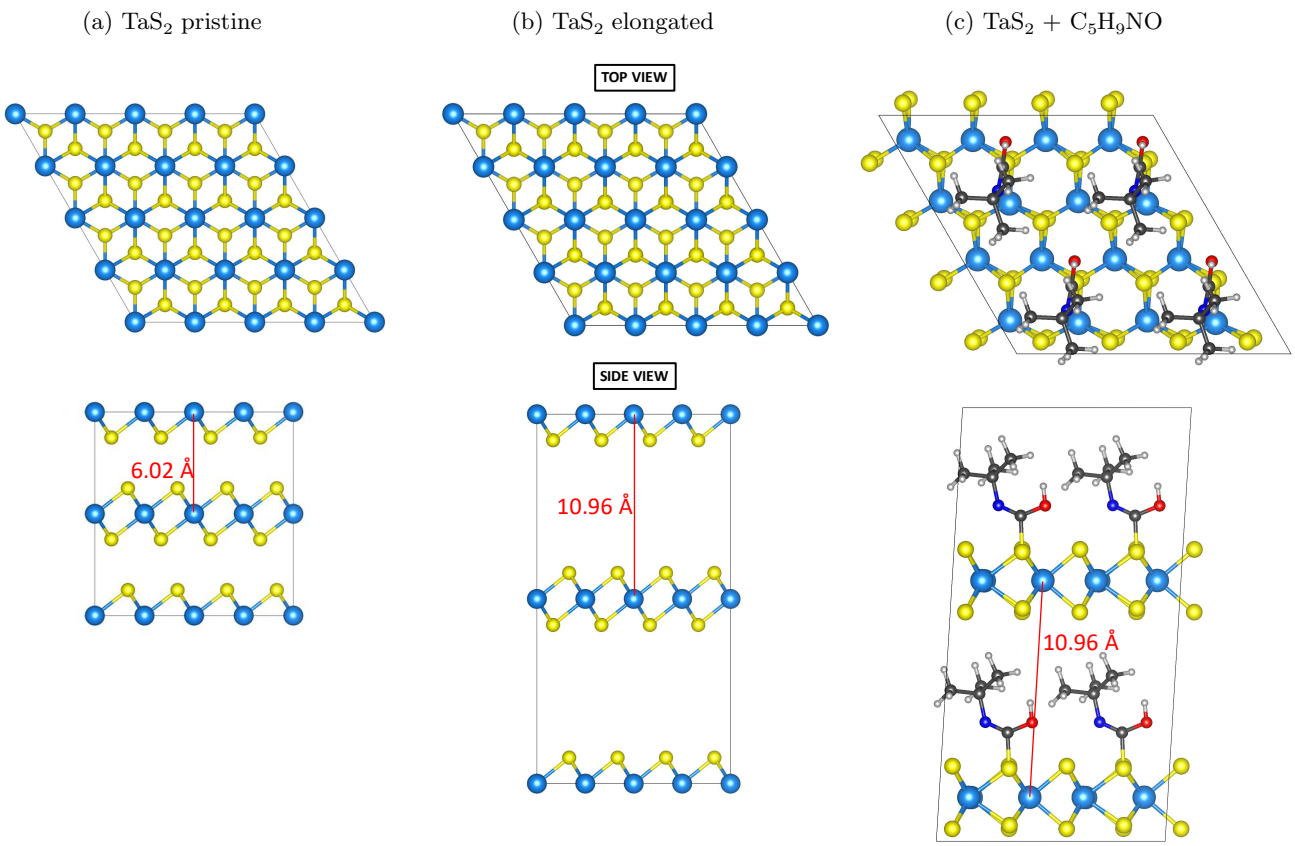

Figure 1: Stick and balls representation of the three geometry optimized structures under study: *a*) bulk TaS_2; *b*) elongated TaS_2 and *c*)TaS_2+tert-Butyl isocyanate.

ing experimental values (see Tab.1).
In order to obtain the structure (*c*), we started from the optimized structure (*a*), and we manually introduced the tert-Butyl isocyanate molecules, ensuring an initial C-S distance of 3 Å. The experimental procedure used to induce the formation of a covalent bond between tert-Butyl isocyanate and TaS_2 has been in fact rather complex [16]. Initially, electrochemical reduction charged TaS_2, followed by electron doping to enhance sulfur atom reactivity. This facilitated the binding of sulfur atoms with the carbon atom of isocyanates, forming covalent bonds. As a matter of fact, reproducing such a complex chemistry is out-of-reach of the theoretical framework here adopted (and, likely, in any case overwhelmingly heavy as for the corresponding computational workload); therefore, we opted for an alternative method to induce the formation of an S-C covalent bond. Specifically, we functionalized the oxygen atom of the isocyanate group by adding an extra hydrogen atom. This functionalization effectively reduced the double bond character of the C=O bond, thereby facilitating the creation of the corresponding C-S covalent bond. Since we had no information of the concentration of the molecules, we assumed the highest concentration possible, namely one tert-Butyl isocyanate molecule every 4 TaS_2 unit cells. The final structure after the geometry optimization show an inter-layer distance (see Tab.1) as large as 10.96 Å, which is in very good agreement with the experimental value of 10.36 Å. The C-S distance is found to be 1.8 Å (similar to the typical length of C-S bonds of 1.7 Å), which indicates the creation of a covalent bond. The closest distance between the H atoms of the tert-butyl isocyanate and the S atoms of TaS_2 is 3.25 Å, far exceeding the typical length of S-H bonds (as short as 1.4 Å). Additionally, we observed a slight variation in the supercell angle α, although this variation is minimal, being less than 1%. Finally, structure (*b*) was obtained from structure (*c*) by removing the covalently bonded tert-Butyl isocyanate molecules, and performing an internal geometry optimization while keeping the supercell volume fixed.
In Figure 2, we display the calculated phonon dispersion relations for structures (*a*), (*b*), and (*c*), color-coded according to their respective phonon lifetimes. In both system (*a*) and (*b*), since we have six atoms

Table 1: Calculated inter-layer separation and tilting angle compared to the corresponding experimental values for the (a) and (c) structures.

System	Inter-layer separation (Exp [16])	α
TaS_2 Bulk	6.02 (6.03) Å	90.00°
TaS_2 + C_5H_9NO	10.96 (10.36) Å	89.24°

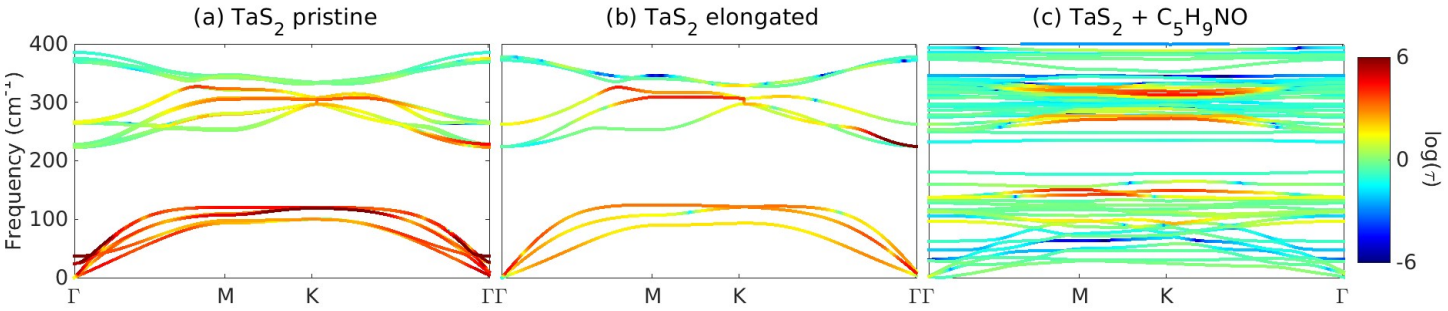

Figure 2: Phonon dispersion relations. Color code (right) showing their respective lifetimes for the three systems under study (a log scale is used for phonon lifetimes).

per unit cell (three atoms per layer), we have a total of 18 dispersion curves, 3 acoustic and 15 optical. In system (c) there are 29 atoms per unit cell, therefore we have a total of 87 dispersion curves (3 acoustic and 84 optical).

As variance with structures (b) and (c), in structure (a) we observe three low-frequency optical phonon branches, denoted as quasi-acoustic modes because of their strong similarities with the corresponding acoustic modes [24]. Such quasi-acoustic branches have been identified in numerous layered and 2D materials and are attributed to the weak interactions between layers [25, 26, 27, 28]. In the case of TaS_2, these quasi-acoustic branches are related to specific inter-layer shear phonon modes (see Figure 3) and are dominated by the van der Walls interactions. The presence of quasi-acoustic branches has two consequences: 1) they provide a sizable contribution to the lattice thermal conductivity in addition to the acoustic branches, and 2) they can scatter with acoustic phonons. While the former effect enhances thermal conductivity, the latter lowers it.

In structure (b), the planes are spaced enough to exhibit negligible van der Waals interactions, thereby hindering the quasi-acoustic shearing modes. For this reason, since the interaction between the layers is now negligible, all the dispersion curves (both acoustic and optical) are now two times degenerate showing a total of nine visible phonon branches. Besides the disappearance of the quasi-acoustic phonon modes, the increase in separation alone results in a slight decrease of the phonon lifetimes.

The introduction of tert-Butyl isocyanate (the (c) structure) further diminishes phonon lifetimes and in-

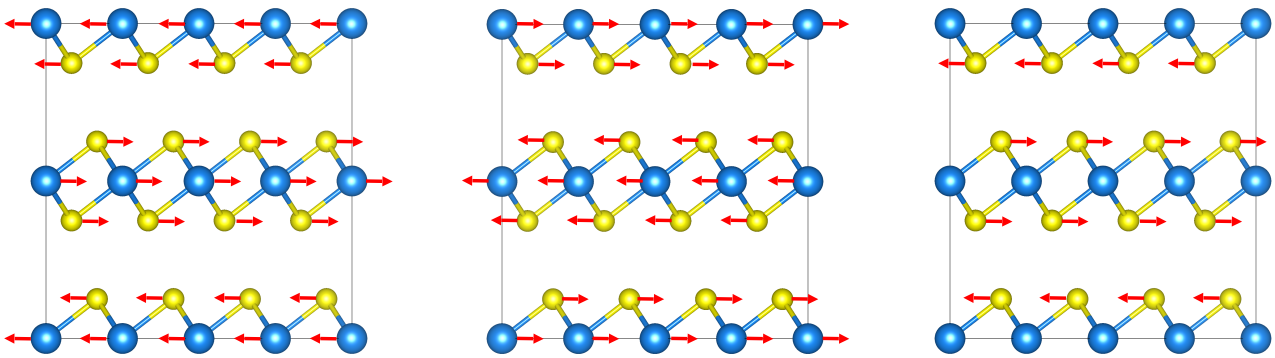

Figure 3: Red arrows visualize the atomic displacements associated with the, first, second and third quasi-acoustic modes in bulk TaS_2.

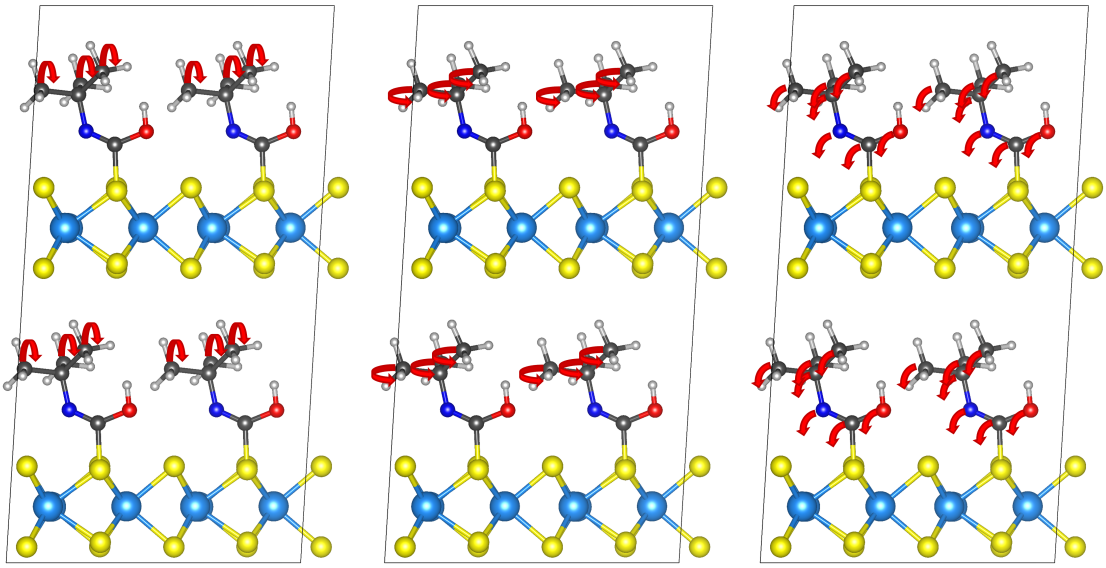

Figure 4: Red arrows visualize the atomic displacements associated with the, first, second and third optical modes in the functionalized system TaS_2 + tert-butyl isocyanate.

duces a significant modification of the dispersion relations. In particular, the introduction of the covalently bonded molecules gives rise to a significant flattening of the TaS_2 acoustic modes. Such an effect is attributed to the presence of nearly dispersionless low-frequency optical molecular modes that cross with the acoustic TaS_2 modes resulting in such a flattening. In Figure 4, we visualized such a low-frequency molecular optical modes by red arrows: the first two modes involve specific rotations of the butyl groups, and the third involves the rotation of the whole tert-butyl isocyanate molecule. The phonon-crossing phenomenon, identified in various structures [29, 30, 31], are usually correlated with a noteworthy decrease in acoustic phonon group velocities and a corresponding strong increases of the vibrational anharmonicity, ultimately resulting in a further decrease of thermal conductivity [32].
Figure 5 shows the corresponding group velocities of the acoustic (and quasi-acoustic for structure (*a*)) phonon modes (see Figure 5). For structures (*a*) and (*b*), we note marginal variations in the group velocities of the acoustic phonon modes. The most noteworthy distinction is evident in the low-frequency ZA mode, characterized by the lowest group velocity, where the elongation further diminishes the group velocity.

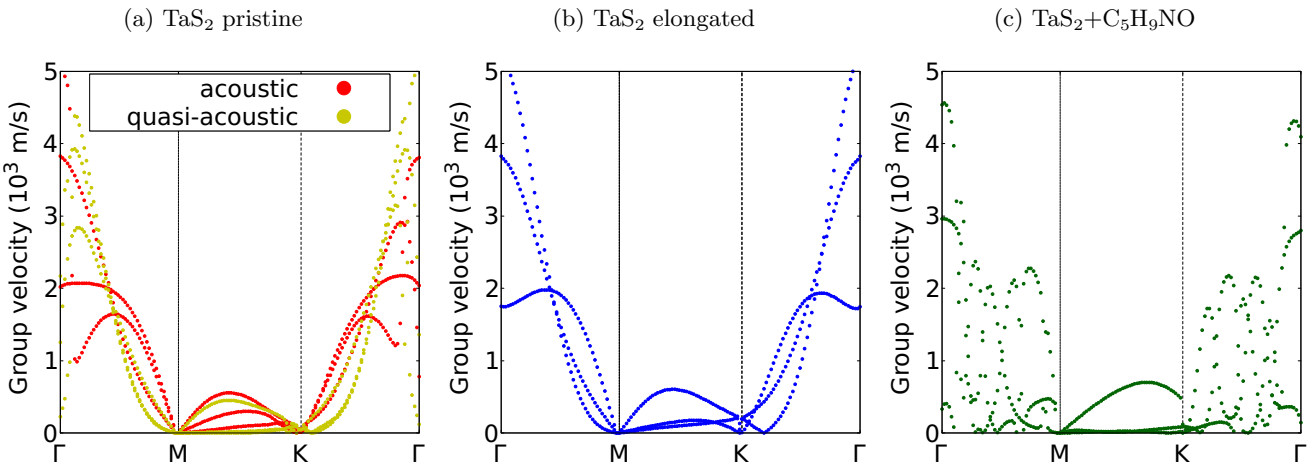

Figure 5: Group velocity of acoustic and quasi-acoustic modes for *a*) bulk TaS_2, *b*) elongated TaS_2 and *c*) TaS_2+C_5H_9NOOS.

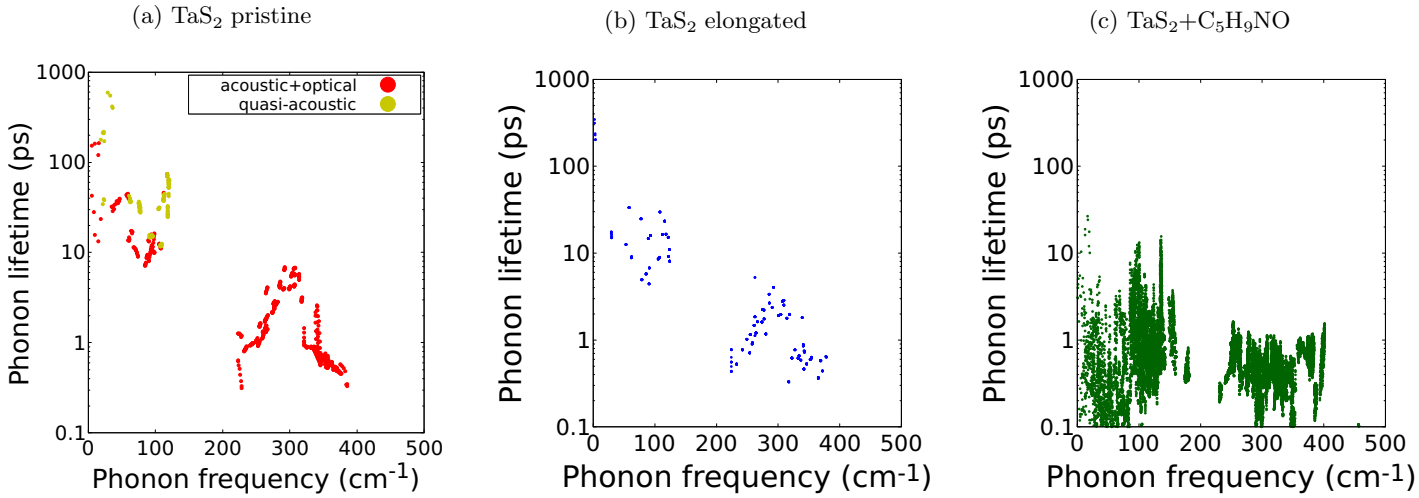

Figure 6: Phonon lifetimes of *a* bulk TaS_2, *b*) elongated TaS_2 and *c*) TaS_2 + C_5H_9NO.

Moreover, as previously mentioned, in the case of the bulk structure we observe that the three quasi-acoustic phonon branches show group velocities comparable to the acoustic ones, therefore we expect a corresponding large contribution to the total lattice thermal conductivity.
Finally, the TaS_2 functionalization with tert-Butyl isocyanate (structure (*c*)), greatly reduces the acoustic group velocities due to the occurrence of phonon-crossing with low-frequency molecular optical modes.
Finally, the TaS_2 functionalization with tert-Butyl isocyanate (structure (*c*)), greatly reduces the acoustic group velocities due to the mixing of molecular optical bands with the acoustic bands.
In Figure 6, we show the corresponding phonon lifetimes. Surprisingly, the highest phonon lifetime in structure (*a*) are the quasi-acoustic ones, with values above 100 ps. This observation, coupled with their high group velocities, suggests that quasi-acoustic modes play a substantial role in the overall bulk lattice thermal conductivity of TaS_2. Besides the quasi-acoustic modes, we observe slight differences in the phonon lifetimes between structures (*a*) and (*b*). As due to the high density of phonon branches upon the introduction of the covalently bonded tert-Butyl isocyanate, we observe a dramatic decrease of all the phonon lifetimes dropping below 50 ps.
Finally, from the information of specific phonon group velocities and lifetimes, we can estimate the lattice thermal conductivity (κ) by Equation (1). Figure 7 shows the estimated thermal conductivities as function of temperature in the range 200 K $\leq T \leq$ 500 K for structure (*a*) (red line), (*b*) (blue line) and (*c*) (green line). Black dots represent the corresponding experimental values [16]. Since the reported experimental values in Ref. [16] referred to the total (lattice+electronic) thermal conductivity, we extract the corresponding lattice thermal conductivity by subtracting the electronic contribution (as large as $\approx 10\%$ for pristine TaS_2 and $\approx 89\%$ for TaS_2 + C_5H_9NO), estimated via the Wiedemann-Franz law, from the experimentally reported total thermal conductivity [16].

Table 2: Thermal conductivity at 300 K ($Wm^{-1}K^{-1}$).

System	Calculated	Experimental [16]
TaS_2 Bulk	37.03	36.00
TaS_2 elongated	17.35	- -
TaS_2 + C_5H_9NO	0.19	0.60

Table 2 shows the the thermal conductivity values estimated at 300 K in comparison with the experimental values.
The calculated values are in very strong agreement with the experiments with a discrepancy at 300 K as small as 3%. This excellent agreement provides a robust validation of the accuracy of all the methodologies used in estimating lattice thermal conductivities. A deviation of about 5 % from the experiments is observed for temperatures above 300 K. We attribute these deviations to the use of a constant Lorentz

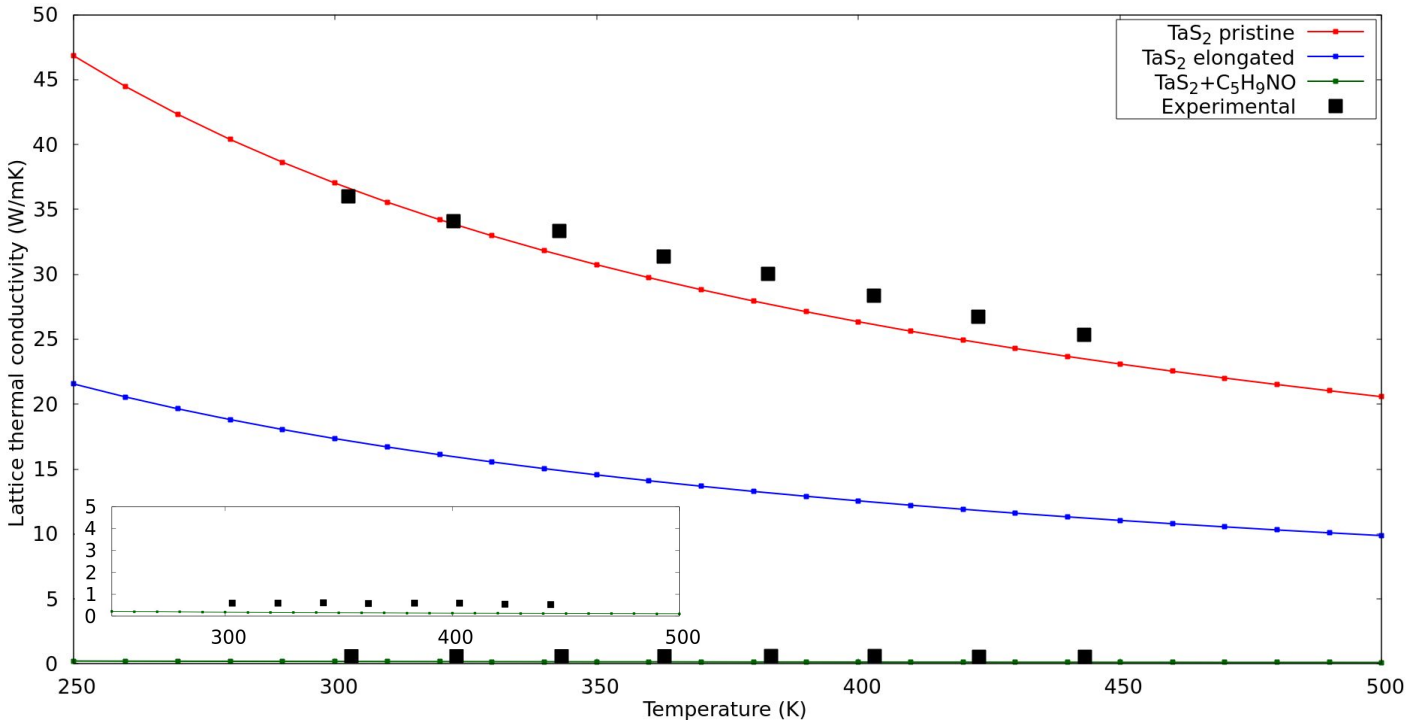

Figure 7: In-plane thermal conductivity of every system in respect of the temperature. The inset emphasizes the comparison between the estimated thermal conductivity and the experimental values for TaS_2 + C_5H_9NO.

number in the Wiedemann-Franz law to determine the electronic contribution to overall thermal conductivity. It has been shown that the Lorentz number can exhibit slight temperature dependence [33]. Therefore, taking this temperature dependency into account could lead to a reduction in uncertainty with respect to the experiments.

From Figure 7 we observe that the inter-layer separation increase induced by the presence of the molecules, from 6.02 Å (structure (a)) to 10.96 Å (structure (b)), significantly decreases the lattice thermal conductivity from 37.03 $Wm^{-1}K^{-1}$ down to 17.35 $Wm^{-1}K^{-1}$. As mentioned above, we attribute such an important decrease to the disappearance of the quasi-acoustic phonon modes due to the reduction of the inter-layer Van der Walls interactions. These modes exhibited notable group velocities and the longest phonon lifetimes, thus making a substantial contribution to the lattice thermal conductivity in Equation (1). This result deviates from conventional findings in well-explored systems like graphene [**?**, 20, 34] or BN mono-layers [21], where increasing inter-layer separation typically leads to an increase in thermal conductivity.

Explicitly considering the presence of the covalently bonded tert-Butyl isocyanate molecule leads to a noteworthy additional reduction in lattice thermal conductivity, down to 0.2 $Wm^{-1}K^{-1}$. In addition to the previously described impact of inter-layer separation, this further decrease is attributed to the combined effects of a significant reduction in acoustic phonon group velocities, as previously described, and a substantial reduction in phonon lifetimes. The estimated lattice thermal conductivity slightly underestimates the experimental value of 0.6 $Wm^{-1}K^{-1}$. We attribute such a slight discrepancy to the molecular coverage that we assumed in our simulations. As mentioned before, since the actual molecular coverage was not explicitly stated in Ref. [16], we adopted the assumption of the maximum obtainable molecular coverage. We expect that such a a high molecular coverage might extensively affect the lattice thermal conductivity.

In order to further characterize the contribution of specific frequencies on the lattice thermal conductivity, we report in Figure 8 (left) the spectral thermal conductivity of all the structures and in Figure 8 (right) the corresponding cumulative normalized thermal conductivity. We observe that in the (a) and (b) structures considered, the main contribution ($\approx 90\%$) is attributed to relatively low frequency modes

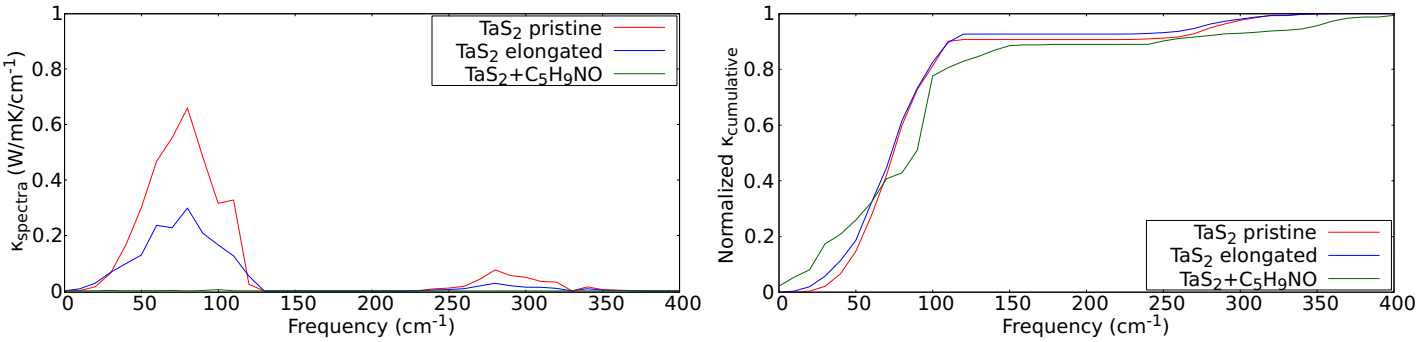

(a) (b)

Figure 8: a) Thermal conductivity spectrum b) Cumulative thermal conductivity

below 100 cm^{-1}. In the case of the (c) structure, we observe that higher frequency modes extending up to 150 cm^{-1} play a significant role in affecting the lattice thermal conductivity. This is attributed to the abundance of optical modes within the 100 to 150 cm^{-1} range. Despite exhibiting only a modest group velocity, these modes possess a non-negligible lifetime, thus making an additional contribution to the total thermal conductivity.

The decomposition of the thermal conductivity among acoustic, quasi-acoustic and optical contributions is reported in Figure 9. We observe that for the bulk structure, the contribution of quasi-acoustic modes ($\approx$ 55%) is predominant over acoustic ($\approx$ 35%) and optical ($\approx$ 15%) modes. In terms of absolute numbers the acoustic modes give a contribution to the thermal conductivity of $\approx$ 14 $Wm^{-1}K^{-1}$. By increasing the inter-layer distance, almost all the contribution (larger than 90%) is attributed to acoustic modes which in terms of absolute numbers represent a κ contribution of $\approx$ 15 $Wm^{-1}K^{-1}$. This gives evidence of two phenomena: 1) the disappearance of the quasi-acoustic contribution is the main reason for the decrease in the thermal conductivity induced by the increase in the inter-layer separation; 2) the effect of the increased phonon scattering due to the presence of quasi-acoustic modes slightly lowers the thermal conductivity contribution due to acoustic modes by $\approx$ 1 $Wm^{-1}K^{-1}$

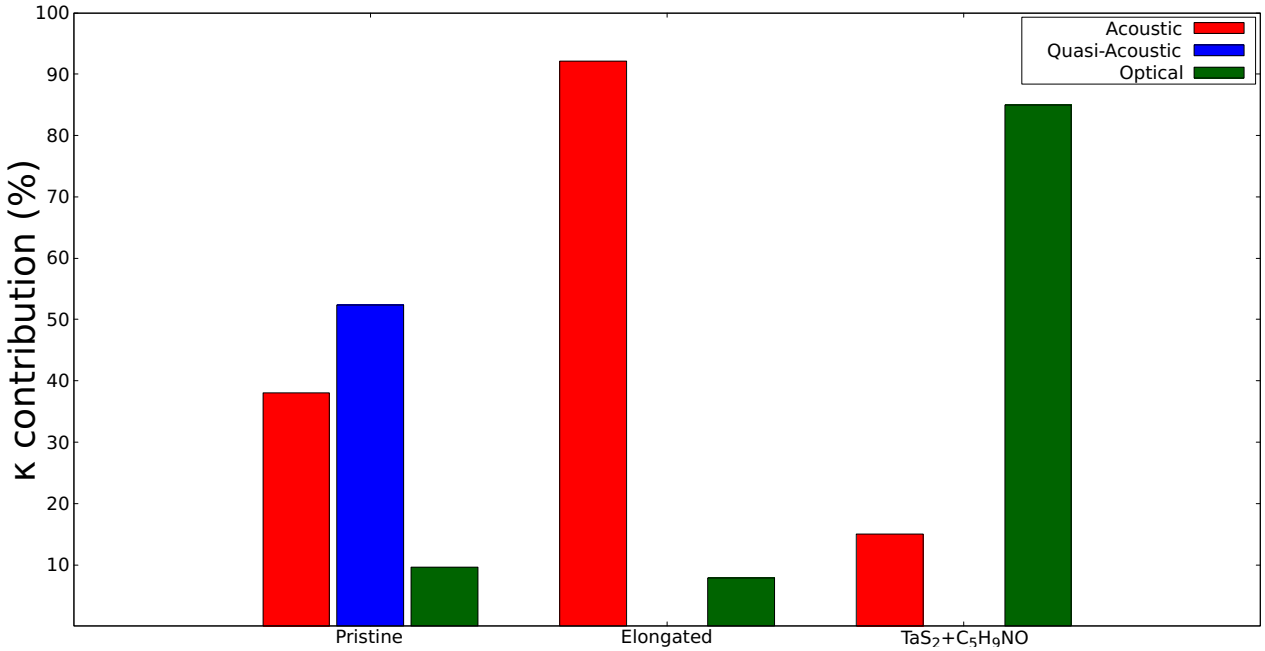

Figure 9: Acoustic, quasi-acoustic and optical contributions to thermal conductivity for the systems of interest

3 Conclusion

In conclusion, by a fully ab initio investigation we have thoroughly characterized both the harmonic and 3rd order anharmonic properties of bulk TaS_2 functionalized with C_5H_9NO. This specific functionalization has been experimentally demonstrated to induce a remarkable reduction in lattice thermal conductivity as high as 98%. To provide insights into these experimental observations, we performed thorough calculations by analyzing the phonon dispersion relations and scattering rates in both pristine and functionalized TaS_2.
We observed two notable structural effects as due to the molecular functionalization: a significant increase in the inter-layer distance, from 6.03 Å up to 10.36 Å and the formation of a covalent C-S bond between C_5H_9NO and TaS_2. The interlayer separation increase is intrinsically responsible for a thermal conductivity reduction of ≈53% with respect to pristine pristine bulk TaS_2. Such a reduction is due to the suppression of specific interlayer shearing quasi-acoustic modes that significantly contribute to the bulk thermal conductivity. Additionally, the effect of covalently bonded C_5H_9NO molecules is to introduce low frequency molecular optical modes which, due to phonon crossing with pristine TaS_2 acoustic modes, cause an overall reduction of phonon group velocities as well as lifetimes. These reductions lead to an additional decrease in thermal conductivity by approximately ≈46% of the bulk thermal conductivity, contributing to an overall reduction of roughly ≈99%. Thus, it is evident that both factors significantly contribute to the notable decrease in observed thermal conductivity.

4 Computational section

4.1 Theory

The thermal transport properties of both pristine and functionalized TaS_2 were summarized by their thermal conductivity κ which was provided by the Boltzmann Transport Equation in Relaxation Time Approximation (BTE-RTA) [35]:

$$\kappa_{\alpha,\beta} = \frac{1}{N_{\mathbf{q}} V} \sum_{\boldsymbol{qj}} \hbar \omega_{\boldsymbol{qj}} v_{\boldsymbol{qj},\beta} v_{\boldsymbol{qj},\alpha} \tau_{\boldsymbol{qj}} \frac{\partial n^{BE}_{\boldsymbol{qj}}}{\partial T}. \tag{1}$$

where the sum is over all the phonon branches j and the $\mathbf{q}$-points in the First Brillouin Zone, the corresponding mesh contains as many as $N_{\mathbf{q}}$ points. This expression depends on the phonon frequency $\omega_{\boldsymbol{qj}}$, on the Cartesian α and β components of the phonon group velocity $v_{\boldsymbol{qj}}$, on the phonon lifetimes $\tau_{\boldsymbol{qj}}$ and on the derivative of the Bose-Einstein distribution $n^{BE}_{\boldsymbol{qj}}$ with respect to temperature T. The various $\omega_{\boldsymbol{qj}}$ used in Equation (1) are obtained with a pure harmonic approximation, while the $\tau_{\boldsymbol{qj}}$ are obtained using a third order anharmonicity, since three-phonon process usually play the prevalent role in thermal transport phenomena. This is a standard approach for this kind of calculations and proof of its efficacy in this specific case will be provided below.

4.2 Computational protocol

All calculations presented in this study rely on Density Functional Theory (DFT) and had been performed using three different model systems: *a*) pristine bulk TaS_2 (see Figure 1, left); *b*) elongated TaS_2 (i,e., bulk TaS_2 with an expanded inter-layer distance, see Figure 1, center); and *c*) functionalized TaS_2 (bulk TaS_2 with both an enlarged inter-layer distance and the explicit incorporation of covalently bonded tert-Butyl isocyanate molecules, see Figure 1, right). Hereafter, the three systems would be referred as structure (*a*), (*b*) and (*c*), respectively. All the DFT calculations were performed in periodic boundary conditions and implemented in the Quantum Espresso package [36]. The corrected generalized gradient approximation of Perdew, Burke and Ernzehof [37], PBEsol [38], was used in all calculations with Projector-Augmented Wave (PAW) pseudopotentials [39] and a plane-wave basis set. In all calculations, a plane-wave cutoff of 60 Ry and a charge-density cutoff of 480 Ry was adopted. The force conver-

gence criterion was set to 10^{-12} Ry/Å and the energy convergence criterion was set to 10^{-15} Ry. In all the three cases the k-mesh sampling was set to 0.1 $Å^{-1}$.
In order to estimate κ from Equation (1), calculation of $\omega_{\boldsymbol{q}j}$ and $\tau_{\boldsymbol{q}j}$ was needed by estimating the interatomic force constants (IFCs). They were respectively obtained from harmonic IFCs and from 3rd order IFCs. To calculate the IFCs, the finite displacement method using the Alamode package[40] was chosen. In order to evaluate the harmonic IFCs, a conventional hexagonal cell obtained as a $4 \times 4 \times 2$ replica of the primitive cell containing 96 atoms for the bulk and elongated systems and 232 atoms for the functionalized TaS_2 system was adopted. In order to reduce the computational cost, that otherwise would be overwhelming, for the 3rd order IFCs calculation the number of replicas was reduced to a $2 \times 2 \times 2$ supercell corresponding to supercells with 24 for the bulk and elongated systems and 58 atoms for the functionalized TaS_2 system.A size effect evaluation was performed for the bulk TaS_2 system and no differences was observed on the results between the $4 \times 4 \times 2$ and the $2 \times 2 \times 2$ supercells.
In the evaluation of the harmonic IFCs of all systems and for the cubic IFCs of pristine and elongated TaS_2, any cutoff for the interatomic interactionshad not been imposed. On the other hand, in order to reduce the computational cost, for the evaluation of 3rd order IFCs for the functionalized TaS_2 system, a cutoff corresponding to the first-neighbors distance was imposed.

Acknowledgements
F. S. acknowledged that this publication was produced while attending the PhD programme in Physics at the University of Cagliari, Cycle XXXVIII, with the support of a scholarship financed by the Ministerial Decree no. 351 of 9th April 2022, based on the NRRP - funded by the European Union - NextGenerationEU - Mission 4 "Education and Research", Component 1 "Enhancement of the offer of educational services: from nurseries to universities" - Investment 4.1 "Extension of the number of research doctorates and innovative doctorates for public administration and cultural heritage". Antonio Cappai and Luciano Colombo acknowledge the financial support under the National Recovery and Resilience Plan (NRRP), Mission 4 Component 2 Investment 1.3 - Call for tender No.341 published on March 13, 2022) by the Italian Ministry of University and Research (MUR) funded by the European Union – NextGenerationEU. Award Number: Project code PE00000021, Concession Decree No. 1561 adopted on October 11, 2022 by the Italian Ministry of Ministry of University and Research (MUR), CUP F53C22000770007, Project title "NEST - Network 4 Energy Sustainable Transition".The authors acknowledged the CINECA award under the ISCRA initiative, for the availability of high-performance computing resources and support.

References

[1] A. K. Kushwaha, H. Kalita, S. Suman, A. Bhardwaj, R. Ghosh, In R. Kumar, R. Singh, editors, *Thermoelectricity and Advanced Thermoelectric Materials*, Woodhead Publishing Series in Electronic and Optical Materials, 233–260. Woodhead Publishing, Cambidge, **2021**.

[2] D. Beretta, N. Neophytou, J. M. Hodges, M. G. Kanatzidis, D. Narducci, M. Martin- Gonzalez, M. Beekman, B. Balke, G. Cerretti, W. Tremel, A. Zevalkink, A. I. Hofmann, C. Müller, B. Dörling, M. Campoy-Quiles, M. Caironi, *Mater. Sci. Eng.: R: Rep.* **2019**, *138* 100501.

[3] V. Shanmugam, R. A. Mensah, K. Babu, S. Gawusu, A. Chanda, Y. Tu, R. E. Neisiany, M. Försth, G. Sas, O. Das, *Particle & Particle Systems Characterization* **2022**, *39*, 6 2200031.

[4] E. A. Marseglia, *International Reviews in Physical Chemistry* **1983**, *3*, 2 177.

[5] R. M. A. Lieth, J. C. J. M. Terhell, *Transition Metal Dichalcogenides*, 141–223, Springer Netherlands, Dordrecht, **1977**.

[6] M. Kang, B. Kim, S. H. Ryu, S. W. Jung, J. Kim, L. Moreschini, C. Jozwiak, E. Rotenberg, A. Bostwick, K. S. Kim, *Nano Letters* **2017**, *17*, 3 1610.

[7] X. Wen, Z. Gong, D. Li, *InfoMat* **2019**, *1*, 3 317.

[8] M. M. Perera, M.-W. Lin, H.-J. Chuang, B. P. Chamlagain, C. Wang, X. Tan, M. M.-C. Cheng, D. Tománek, Z. Zhou, *ACS Nano* **2013**, *7*, 5 4449.

[9] B. Radisavljevic, A. Radenovic, J. Brivio, V. Giacometti, A. Kis, *Nature Nanotechnology* **2011**, *6*, 3.

[10] J. Kumar, M. A. Kuroda, M. Z. Bellus, S.-J. Han, H.-Y. Chiu, *Applied Physics Letters* **2015**, *106*, 12 123508.

[11] Y. Yu, T. Minhaj, L. Huang, Y. Yu, L. Cao, *Phys. Rev. Appl.* **2020**, *13* 034059.

[12] J. Guo, F. Yang, M. Xia, X. Xu, B. Li, *Journal of Physics D: Applied Physics* **2019**, *52*, 38 385306.

[13] M. R. Jobayr, E. M.-T. Salman, *Chinese J. Phys.* **2021**, *74* 270.

[14] R. Yan, J. R. Simpson, S. Bertolazzi, J. Brivio, M. Watson, X. Wu, A. Kis, T. Luo, A. R. Hight Walker, H. G. Xing, *ACS Nano* **2014**, *8*, 1 986, pMID: 24377295.

[15] Y. Hong, J. Zhang, X. C. Zeng, *The Journal of Physical Chemistry C* **2016**, *120*, 45 26067.

[16] S. Wang, L. Hou, X. Cui, X. Zheng, J. Zheng, *Nature Communications* **2022**, *12*, 1.

[17] Z. Yan, C. Jiang, T. R. Pope, C. F. Tsang, J. L. Stickney, P. Goli, J. Renteria, T. T. Salguero, A. A. Balandin, *Journal of Applied Physics* **2013**, *114*, 20 204301.

[18] E. Selezneva, A. Vercouter, G. Schweicher, V. Lemaur, K. Broch, A. Antidormi, K. Takimiya, V. Coropceanu, J.-L. Brédas, C. Melis, J. Cornil, H. Sirringhaus, *Advanced Materials* **2021**, *33*, 37 2008708.

[19] M. N. Gueye, A. Vercouter, R. Jouclas, D. Guérin, V. Lemaur, G. Schweicher, S. Lenfant, A. Antidormi, Y. Geerts, C. Melis, J. Cornil, D. Vuillaume, *Nanoscale* **2021**, *13* 3800.

[20] P. Klemens, D. Pedraza, *Carbon* **1994**, *32*, 4 735.

[21] V. Guerra, C. Wan, T. McNally, *Progress in Materials Science* **2019**, *100* 170.

[22] X. Wei, Y. Wang, Y. Shen, G. Xie, H. Xiao, J. Zhong, G. Zhang, *Applied Physics Letters* **2014**, *105*, 10 103902.

[23] X. Zhang, D. Sun, Y. Li, G.-H. Lee, X. Cui, D. Chenet, Y. You, T. F. Heinz, J. C. Hone, *ACS Applied Materials & Interfaces* **2015**, *7*, 46 25923.

[24] G. Liu, Z. Zhang, H. Wang, G.-L. Li, J.-S. Wang, Z. Gao, *Journal of Applied Physics* **2021**, *130*, 10 105106.

[25] J. L. Verble, T. J. Wieting, *Physical Review Letters* **1970**, *25* 362.

[26] A. N. Gandi, U. Schwingenschlögl, *Europhysics Letters* **2016**, *113*, 3 36002.

[27] X. Zhang, X.-F. Qiao, W. Shi, J.-B. Wu, D.-S. Jiang, P.-H. Tan, *Chemical Society Reviews* **2015**, *44* 2757.

[28] P. H. Tan, W. P. Han, W. J. Zhao, Z. H. Wu, K. Chang, H. Wang, Y. F. Wang, N. Bonini, N. Marzari, N. Pugno, G. Savini, A. Lombardo, A. C. Ferrari, *Nature Materials* **2012**, *11* 294–300.

[29] M. Christensen, A. B. Abrahamsen, N. B. Christensen, F. Juranyi, N. H. Andersen, K. Lefmann, J. Andreasson, C. R. H. Bahl, B. B. Iversen, *Nature Materials* **2008**, *7* pages811–815.

[30] W. Li, J. Carrete, G. K. H. Madsen, N. Mingo, *Physical Review B* **2016**, *93* 205203.

[31] Y. Li, S. Yamamoto, K. Ahmad, Z. Almutairi, K. Koumoto, C. Wan, *J. Mater. Chem. A* **2021**, *9* 11674.

[32] K. R. Hahn, C. Melis, F. Bernardini, L. Paulatto, L. Colombo, *The Eur. Phys. J. Plus* **2023**, *11*.

[33] G. Catelani, *Physical Review B* **2007**, *75*, 2 024208.

[34] A. A. Balandin, S. Ghosh, W. Bao, I. Calizo, D. Teweldebrhan, F. Miao, C. N. Lau, *Nano Letters* **2008**, *8*, 3 902.

[35] L. Lindsay, *Nanoscale and Microscale Thermophysical Engineering* **2016**, *20*, 2 67.

[36] P. Giannozzi, S. Baroni, N. Bonini, M. Calandra, R. Car, C. Cavazzoni, D. Ceresoli, G. L. Chiarotti, M. Cococcioni, I. Dabo, A. D. Corso, S. de Gironcoli, S. Fabris, G. Fratesi, R. Gebauer, U. Gerstmann, C. Gougoussis, A. Kokalj, M. Lazzeri, L. Martin-Samos, N. Marzari, F. Mauri, R. Mazzarello, S. Paolini, A. Pasquarello, L. Paulatto, C. Sbraccia, S. Scandolo, G. Sclauzero, A. P. Seitsonen, A. Smogunov, P. Umari, R. M. Wentzcovitch, *Journal of Physics: Condensed Matter* **2009**, *21*, 39 395502.

[37] M. Ernzerhof, G. E. Scuseria, *The Journal of Chemical Physics* **1999**, *110*, 11 5029.

[38] J. P. Perdew, A. Ruzsinszky, G. I. Csonka, O. A. Vydrov, G. E. Scuseria, L. A. Constantin, X. Zhou, K. Burke, *Physical Review Letters* **2008**, *100*, 13.

[39] G. Kresse, D. Joubert, *Physical review B* **1999**, *59*, 3 1758.

[40] T. Tadano, Y. Gohda, S. Tsuneyuki, *Journal of Physics: Condensed Matter* **2014**, *26*, 22 225402.